Modified empirical parametrization of fragmentation cross sections

K. Sümmerer[1,*] and B. Blank[2,†]
[1]*Gesellschaft für Schwerionenforschung, Planckstrasse 1, D-64291 Darmstadt, Germany*
[2]*CEN Bordeaux-Gradignan, Le Haut-Vigneau, F-33175 Gradignan Cedex, France*
(Received 27 July 1999; published 14 February 2000)

New experimental data obtained mainly at the GSI/FRS facility allow one to modify the empirical parametrization of fragmentation cross sections. It will be shown that minor modifications of the parameters lead to a much better reproduction of measured cross sections. The most significant changes refer to the description of fragmentation yields close to the projectile and of the memory effect of neutron-deficient projectiles.

PACS number(s): 25.70.Mn, 25.70.Pq, 25.75.−q

I. INTRODUCTION

The pioneering experiments of projectile fragmentation at relativistic energies of ^{40}Ar and ^{48}Ca beams at the LBL Bevalac [1,2] have demonstrated the potential of this method for the production of exotic nuclei. Based on these ideas, the SIS/FRS facility [3] at GSI has used also heavier projectiles like, e.g., ^{58}Ni, ^{86}Kr, ^{129}Xe, and ^{208}Pb to produce and study exotic nuclei [4–7]. For planning such experiments, when count-rate predictions are needed, analytical descriptions of fragmentation cross sections are useful. They are also useful in simulation programs for projectile-fragment separators (like, e.g., INTENSITY [8] or MOCADI [9]). Compared to physical models of high-energy fragmentation reactions, which in general involve time-consuming Monte Carlo calculations, the virtue of an analytical formula lies in the short computing time and the possibility to calculate easily submicrobarn cross sections that are beyond the reach of physical-model calculations.

In 1990, Sümmerer *et al.* [10] proposed a universal empirical parametrization of fragmentation cross sections (EPAX [10]) which was based on and similar to previous prescriptions by Rudstam [11] and Silberberg and Tsao [12]. The parametrization was to a large extent based on multi-GeV proton-induced spallation cross sections, since only scarce heavy-ion-induced experimental data were available at that time. Meanwhile, more precise data from relativistic heavy-ion-induced fragmentation reactions together with recent results from projectile fragmentation of heavy nuclei (^{197}Au and ^{208}Pb) on H_2 targets [13,14]) allow a more stringent comparison of proton- and heavy-ion-induced isotope distributions. This comparison indicates that for heavy nuclei the two reactions lead to different isotopic distributions, which cannot be obtained from each other just by scaling factors. This can be easily understood since heavy-ion-induced reactions are expected to deposit more excitation energy in a nucleus than proton-induced reactions, making the final product distributions — after evaporation — broader and more neutron deficient. Nevertheless, the data show that in both cases the isotopic yield distributions can be well described by Gaussian-like analytical functions with parameters that vary smoothly as a function of fragment mass [10]. In the present paper, we will base the choice of these parameters exclusively on heavy-ion-induced reaction data.

We will first review briefly the basic characteristics of the EPAX formula and then show which modifications are necessary to improve the accuracy with which the new experimental results can be reproduced. This will be followed by a brief comparison with similar attempts by other authors.

II. EPAX FORMULA

A. Basic characteristics

The basic characteristics of the analytical description of high-energy fragmentation cross sections by the EPAX formula are the following [10].

(i) In the absence of systematic excitation-function measurements of heavy-ion-induced fragmentation reactions, the formula is valid only for the so-called ''limiting fragmentation'' regime, i.e., for projectile energies where the fragmentation yields are no longer energy dependent, at least within the accuracy of the formula (approximately within a factor of 2). This is certainly true for incident energies considerably above the Fermi energy in nuclei ($\approx 40A$ MeV), in particular for the typical SIS energies of $(500–1000)A$ MeV.

(ii) The EPAX formula is meant to describe the fragmentation of medium- to heavy-mass projectiles; nucleon-pickup cross sections are not included. No attempt is made to describe the fragmentation of fissile nuclei. Therefore, the range of validity is limited to projectiles from around argon to below the lead and bismuth isotopes. Predictions for production cross sections of fission products or of fragments below U where fission competition is significant require an elaborate description of the fission process, such as can be found, e.g., in a recent publication by Benlliure *et al.* [15].

(iii) For fragments sufficiently far away from the projectile (i.e., for mass losses larger than 15–20 % of the projectile mass), the isotope distributions are largely independent of the original nucleus; their position, shape, and width depend only on the fragment mass number. This constitutes what has been termed the ''residue corridor'' and is related to the fact that the isotope distributions are mainly governed by statistical evaporation from highly excited prefragments produced in collisions between relativistic heavy ions.

(iv) For fragments that involve only a small mass loss from the projectile, the isotope distributions should be cen-

*Electronic address: k.suemmerer@gsi.de
†Electronic address: blank@cenbg.in2p3.fr

TABLE I. Constants used in the EPAX formula version 1 (Ref. [10]) and those used in version 2 (this work). Note that in a few cases also the functional form to calculate a parameter has changed (see text).

Parameter	Constant	Value	
		Version 1	Version 2
Scaling factor S	S_1	-2.38	-2.38
	S_2	0.450	0.270
Mass yield slope P	P_1	-2.584	-2.584
	P_2	-7.57×10^{-3}	-7.57×10^{-3}
Width parameter R	R_1	0.778	0.885
	R_2	-6.77×10^{-3}	-9.82×10^{-3}
Z_{prob} shift Δ	Δ_1	0.895	-1.09
	Δ_2	2.70×10^{-2}	3.05×10^{-2}
	Δ_3	2.04×10^{-4}	2.14×10^{-4}
	Δ_4	66.22	71.35
n-rich slope U_n	U_n	1.50	1.65
p-rich slope U_p	U_1	2.00	1.79
	U_2		4.72×10^{-3}
	U_3		-1.30×10^{-5}
n-rich memory effect Δ_m	n_1	0.40	0.40
	n_2	0.60	0.60
p-rich memory effect Δ_m	p_1	0.00	-10.25
	p_2	0.60	10.10
Correction factor for Δ	d_1	-51.0	-25.0
	d_2	0.86	0.80
Correction factor for R	r_1	20.0	20.0
	r_2	0.86	0.82
Correction factor for Y_A	y_1		200.0
for Y_A	y_2		0.90

tered close to the projectile and their variance should be small. Therefore, a smooth transition is anticipated between the residue corridor and the projectile. The parametrization of this smooth transition constitutes the main task in designing the formula.

In a first step, a parameter set has been searched for that describes the fragmentation yields from projectiles located close to the line of β stability. In a second step, a modification of the yield distributions due to the neutron or proton excess of projectiles located on the neutron- or proton-rich side of the line of β stability (the ''memory effect'') has been parametrized.

B. Parameters of EPAX version 1

As explained in detail in Ref. [10], the cross section (in barns) of a fragment with mass A and charge Z produced by projectile fragmentation from a projectile (A_p, Z_p) impinging on a target (A_t, Z_t) is written as

$$\sigma(A,Z) = Y_A \sigma(Z_{prob} - Z) = Y_A n \exp(-R|Z_{prob} - Z|^{U_{n(p)}}). \quad (1)$$

The first term Y_A represents the mass yield, i.e., the sum of the isobaric cross sections with fragment mass A. The second term describes the ''charge dispersion,'' the distribution of elemental cross sections with a given mass around its maximum, Z_{prob}. The shape of the charge dispersion is controlled by the width parameter R and the exponent U_n (U_p) on the neutron- (proton-) rich side of the residue corridor. The factor $n = \sqrt{R/\pi}$ simply serves to normalize the integral of the charge dispersion to unity.

The mass-yield curve is taken to be an exponential as a function of $A_p - A$. The slope of this exponential, P, is a function of the projectile mass. An overall scaling factor S accounts for the peripheral nature of fragmentation reactions and therefore depends on the circumference of the colliding nuclei:

$$Y_A = SP \exp[-P(A_p - A)], \quad (2)$$

$$S = S_2(A_p^{1/3} + A_t^{1/3} + S_1)[\mathrm{b}], \quad (3)$$

$$\ln P = P_2 A_p + P_1. \quad (4)$$

The numerical values of the various constants can be found in Table I.

The charge dispersion is characterized by the three parameters R, Z_{prob}, and U. These three parameters are strongly correlated and difficult to obtain uniquely with a least-squares fitting technique. Note that the isobar distributions are not symmetric on the neutron- and proton-rich sides; therefore U has two different values U_p and U_n on the

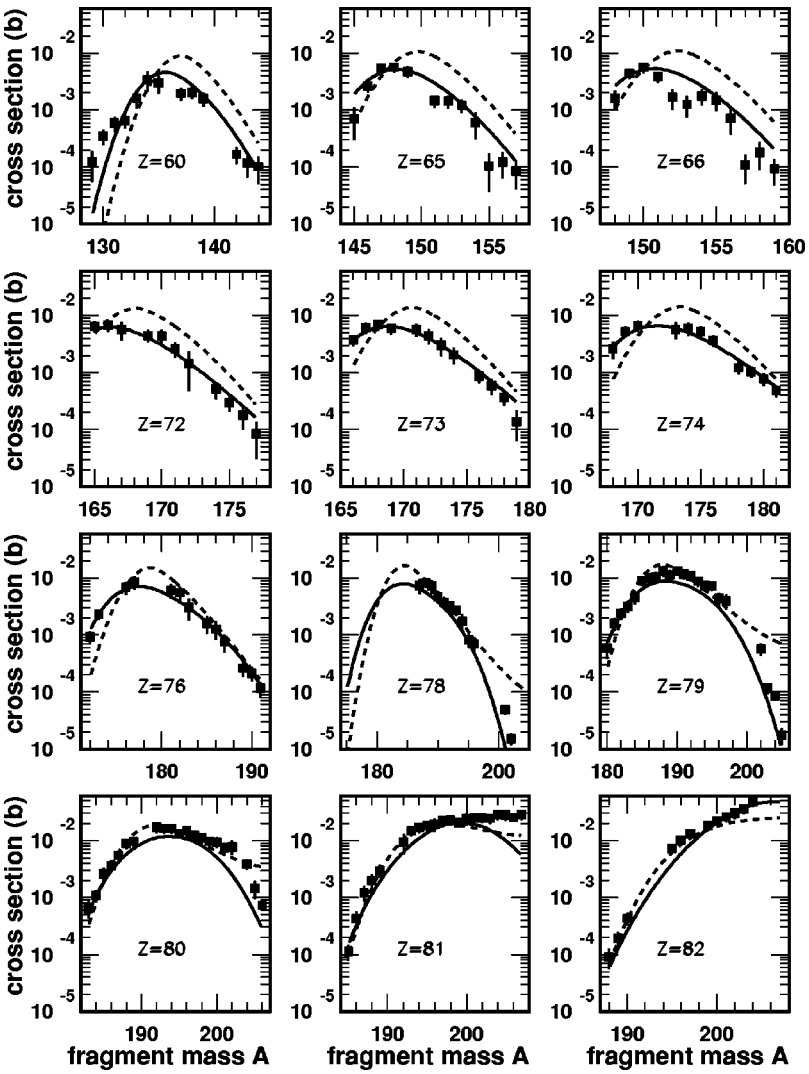

FIG. 1. Isotope distributions from 1*A* GeV ^{208}Pb fragmentation in a ^{nat}Cu target [7] in comparison with the old EPAX parametrization version 1 (dashed curves) and the modified version 2 (solid curves).

proton- or neutron-rich side of the valley of β stability, respectively. In Ref. [10], the exponent U for the neutron-rich side of the isobar distribution was chosen as $U_n=1.5$, whereas the proton-rich side falls off like a Gaussian ($U_p=2$).

The maxima of the charge dispersions, Z_{prob}, have been parametrized relative to the valley of β stability,

$$Z_{prob}=Z_\beta+\Delta. \tag{5}$$

Z_β is approximated by the smooth function

$$Z_\beta=A/(1.98+0.0155A^{2/3}). \tag{6}$$

Δ is found to be a linear function of the fragment mass, A, for heavy fragments ($A\geqslant\Delta_4$), and is extrapolated quadratically to zero:

$$\Delta=\begin{cases}\Delta_3A^2 & \text{if } A<\Delta_4,\\ \Delta_2A+\Delta_1 & \text{if } A\geqslant\Delta_4.\end{cases} \tag{7}$$

Similar to the parameter Z_{prob} just discussed, the width parameter R is a function of fragment mass only, irrespective of the projectile. In Ref. [10] it was found that the experimental R values can be approximated by an exponential of the form

$$\ln R=R_2A+R_1. \tag{8}$$

The equations given above are sufficient to describe the ''residue corridor,'' i.e., the yield distributions of projectiles located on the line of β stability if the fragment mass is far from the projectile mass. Close to the projectile, the following modifications have to be introduced [10]:

$$\Delta=\Delta[1+d_1(A/A_p-d_2)^2], \tag{9}$$

$$R=R[1+r_1(A/A_p-r_2)^2]. \tag{10}$$

This serves to gradually reduce to zero the offset of Z_{prob} from the line of β stability and to decrease the width of the charge dispersion when A approaches the mass of the projectile, A_p.

A final correction applies if the projectile does not lie on the line of β stability. In this case, the A/Z ratio of the fragments will to some extent ''remember'' the A_p/Z_p ratio of the projectile (''memory effect''). For an analytical de-

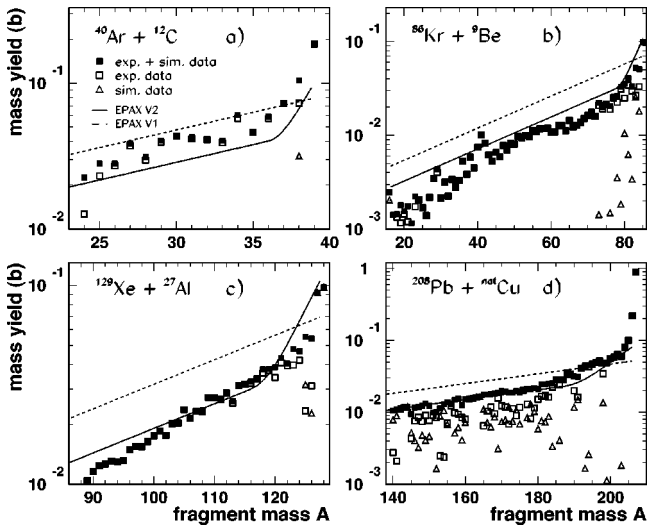

FIG. 2. Experimental mass yields Y_A for the reactions of ^{40}Ar+^{12}C [(a), Ref. [18]], ^{86}Kr+^{9}Be [(b), Ref. [5]], ^{129}Xe+^{27}Al [(c)], Ref. [6]], and ^{208}Pb+^{nat}Cu [(d), Ref. [7]] compared to the old EPAX parametrization version 1 (dashed line) and to the new EPAX formula version 2 (solid line). The open squares are the sum of the experimental cross sections for a given fragment mass *A*, whereas the open triangles represent the calculated cross sections using the new EPAX formula for isotopes missing in the experimental data for a given mass *A*. The solid squares are the sum of the two values.

scription, it is simply assumed that the charge dispersions are shifted by an amount Δ_m which is a certain fraction of the distance of Z_p from $Z_{\beta p}$, the nuclear charge on the line of β stability for A_p. Close to the projectile, this fraction is clearly close to unity (full memory effect), whereas it should gradually approach zero with increasing distance of the fragment mass *A* from the projectile (loss of memory). The shape of the isobar distribution is assumed to be unchanged. Thus

$$Z_{prob} = Z_\beta + \Delta + \Delta_m, \tag{11}$$

where Δ_m for neutron-rich projectiles is given by

$$\Delta_m = [n_1(A/A_t)^2 + n_2(A/A_t)^4](Z_p - Z_{\beta p}). \tag{12}$$

The corresponding constants for proton-rich projectiles are termed p_1 and p_2 instead of n_1 and n_2. Numerical values for all constants are given in Table I.

With this parametrization, EPAX version 1 was rather successful in describing the gross features of isotope distributions of high-energy projectile fragmentation. This has been visualized, e.g., in Refs. [4–7], where comparisons of EPAX with experimental data over many orders of magnitude in cross section can be found. As a particular example, we plot in Fig. 1 experimental isotope distributions from 1*A* GeV ^{208}Pb fragmentation [7] in comparison with the EPAX version 1 parametrization (dashed curves).

This set of data was also chosen to illustrate that the old EPAX version has problems to reproduce satisfactorily the isotope distributions of very heavy fragments. As can be seen best for the low-*Z* isotope distributions, the dashed lines are centered too much on the neutron-rich side and exhibit too large maxima. Moreover, the cross sections for fragments close to the projectile (with masses $A \geqslant 200$) are predicted much too high. Minor discrepancies were also found for ^{129}Xe-fragment yields [6] where the experimental distributions were found to be wider than the EPAX predictions. Serious deficiencies were revealed when, compared to the EPAX prediction, too large cross sections for neutron-deficient isotopes from ^{58}Ni fragmentation [4] and too small cross sections of neutron-deficient Sn isotopes from ^{112}Sn fragmentation [16] were measured.

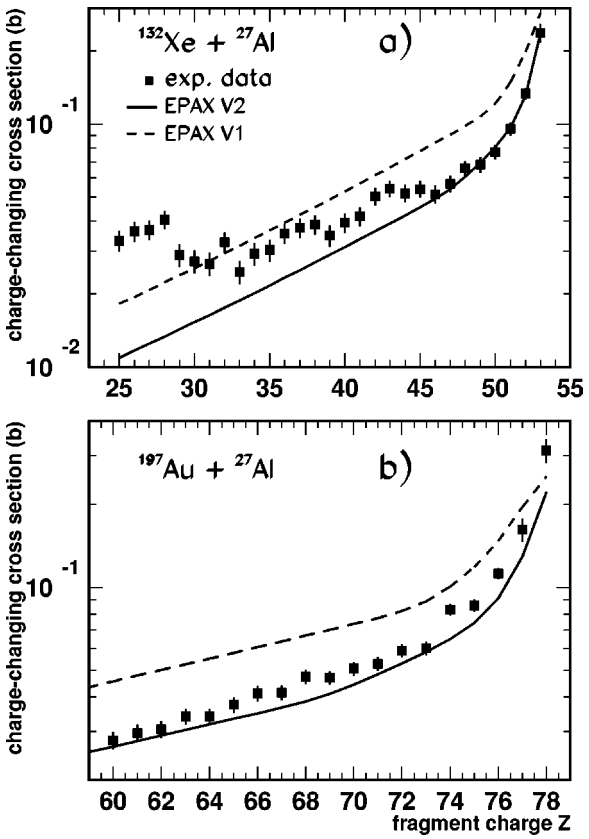

FIG. 3. Experimental charge-changing cross sections for ^{132}Xe (a) and ^{197}Au ions (b) on ^{27}Al targets in comparison with the old EPAX parametrization version 1 (dashed line) and the new EPAX formula version 2 (solid line). The experimental data are from Binns *et al.* [19].

III. MODIFICATIONS OF THE EPAX FORMULA

A. Fragmentation of projectiles close to β stability

The availability of extensive cross-section measurements for projectile fragmentation of ^{40}Ar, ^{58}Ni, ^{86}Kr, ^{129}Xe, and ^{208}Pb [17,4–7] down to μb or nb cross sections allowed in a first step to find a better parametrization of the mass yields Y_A. In a second step, we adjusted the parameters describing the residue corridor, i.e., the width parameter *R* and the slope constants U_n and U_p of the quasi-Gaussian charge dispersion together with its centroid Z_{prob}. In a third step, the correction factors for isotopic yields close to the projectile were modified. Finally, modifications for projectiles outside

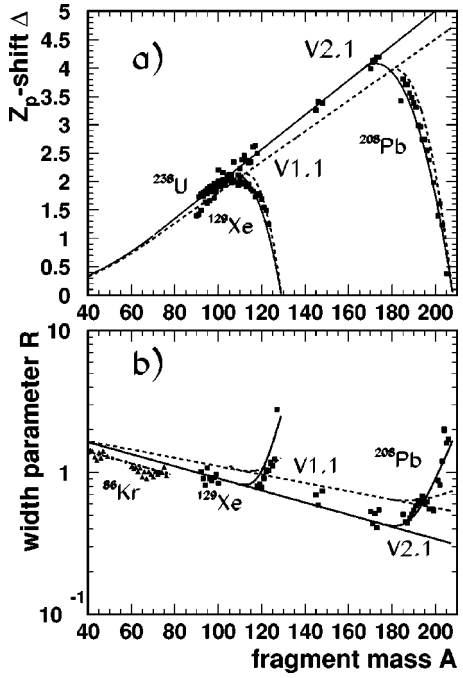

FIG. 4. (a) Fragment-mass dependence of the offset, Δ, of Z_{prob} from the line of β stability according to Eq. (5). The dashed curves denote the old EPAX parametrization, while the modified version 2 is indicated by the solid curves. The downward-curving lines above $A \approx 110$ and $A \approx 180$ illustrate the return of Z_{prob} to β stability close to the projectile [Eq. (9)] for ^{129}Xe and ^{208}Pb, respectively, as a projectile. Data from fits of Eq. (5) to the results from Refs. [6,7,15] are shown by the solid squares. (b) Fragment-mass dependence of the width parameter R according to Eq. (8). The upward-sloping dashed (solid) curves indicate the shrinking of the widths near the ^{129}Xe and ^{208}Pb projectile, respectively, for the old (new) version of EPAX according to Eq. (10) [Eq. (14)]. Results from fits to the data from ^{129}Xe and ^{208}Pb fragmentation are shown by the solid squares; those from ^{86}Kr fragmentation (triangles, Ref. [5]) have been approximated by Eq. (16) (dash-dotted line).

the valley of β stability were redetermined. Numerical values for the new constants are given in the fourth column of Table I.

1. Integrated mass and charge yields

According to Eqs. (2)–(4), Y_A is described by an exponential function depending on the fragment mass A, the projectile mass A_p, and the target mass, A_t. In EPAX version 1, no additional correction close to the projectile has been performed. As shown by the dashed lines in Fig. 2, this yields only a very rough agreement with experimental data. Note that the experimental mass yields had to be complemented by calculated cross sections (from EPAX version 2) where experimental data points were missing. For the ^{40}Ar, ^{86}Kr, and ^{129}Xe data, the additional calculated cross sections contribute only close to the projectile; in the ^{208}Pb case, however, the experimental data are less complete and more significant corrections were necessary.

Figure 2 shows that the slope somewhat further away from the projectile is reasonably well reproduced; however, the absolute height as well as the slope close to the projectile

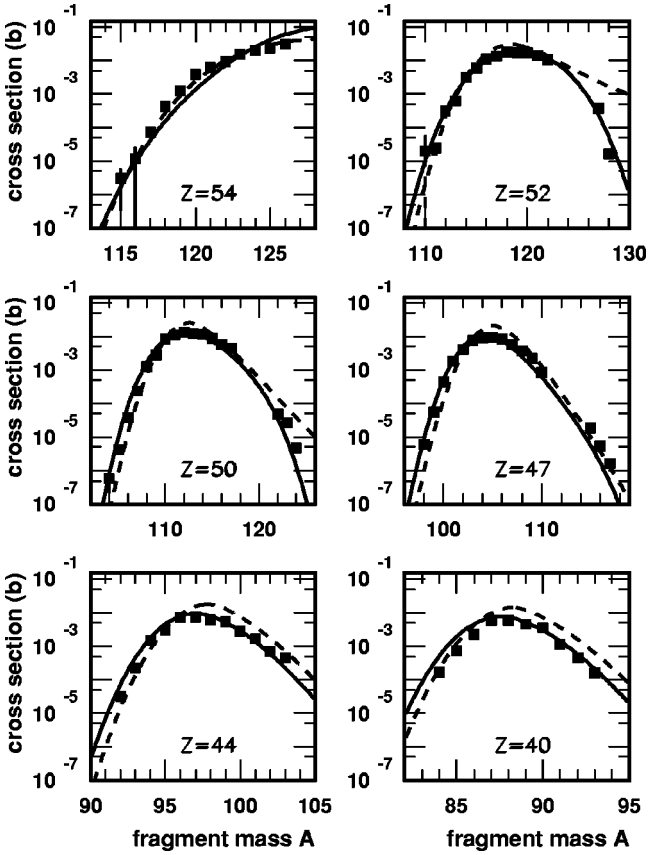

FIG. 5. Isotope distributions from 800A MeV ^{129}Xe fragmentation in a ^{27}Al target [6] in comparison with the old EPAX parametrization version 1 (dashed curve) and the modified version 2 (solid curve).

mass needed to be modified. A much better overall normalization was achieved by reducing the scaling factor S_2 by a factor of 0.6, as demonstrated by the solid lines in Fig. 2. An additional correction introduced in the new EPAX version consists of an increase in the mass yield Y_A [Eq. (2)] close to the projectile according to

$$Y_A = Y_A[1 + y_1(A/A_p - y_2)^2] \tag{13}$$

for $A/A_p \geqslant y_2$. These modifications give a satisfactory agreement with experimental data. In the case of ^{129}Xe, the slope far from the projectile mass deserves further attention. However, because of the lack of other complete experimental data, we were not able to significantly improve the mass-yield description.

Another comparison of integrated cross sections from EPAX to experimental data can be performed for charge-changing cross sections. For this purpose, we use experimental data from Binns *et al.* [19]. Figure 3 shows a comparison of the experimental data to the EPAX versions 1 and 2. As can be seen, nice agreement is achieved with the new EPAX formula, in particular close to the target. For the ^{132}Xe data, the excess charge-changing cross sections for lower Z are most likely due to secondary reactions in the targets which are unsufficiently accounted for.

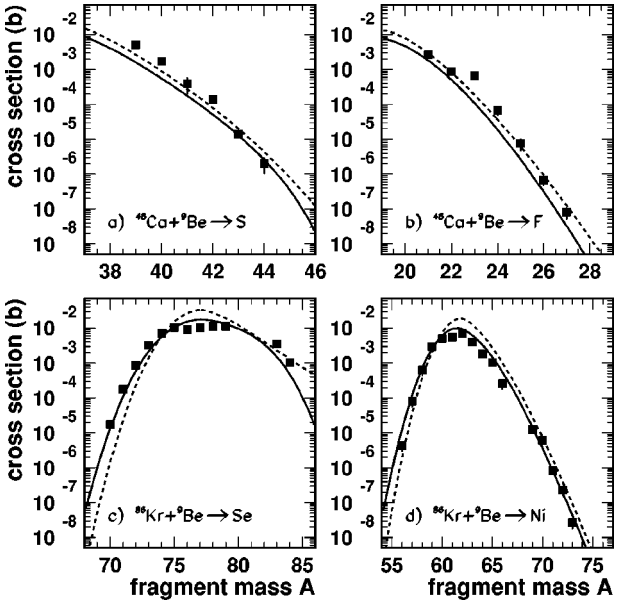

FIG. 6. Examples visualizing the ''memory effect'' for neutron-rich projectiles impinging on ^{9}Be targets. Panels (a) and (b) S and F isotope distributions from ^{48}Ca fragmentation; (c) and (d) Se and Ni isotope distributions from ^{86}Kr fragmentation. The dashed curves are for EPAX version 1, the solid ones for the present version 2. Experimental data are from Refs. [2,5].

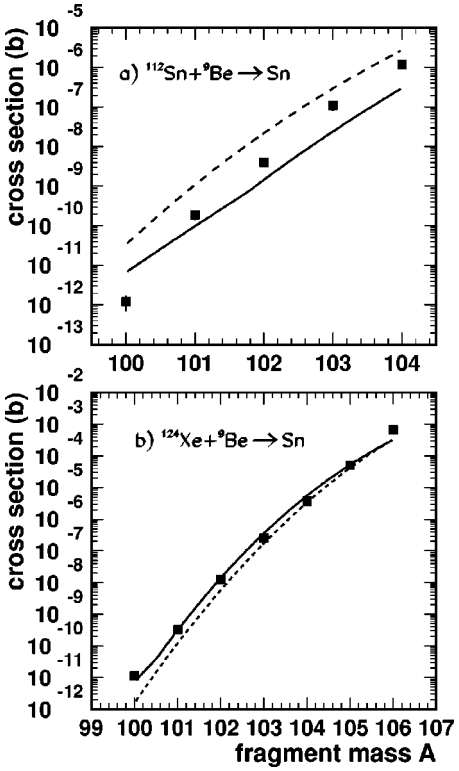

FIG. 7. Experimental isotope distributions for Sn isotopes from neutron-deficient projectiles on ^{9}Be targets: (a) from ^{112}Sn fragmentation [16], (b) from ^{124}Xe fragmentation [21], plotted in comparison with the old EPAX parametrization (dashed curves) and the modified version (solid curves).

2. Parameters of the residue corridor

In the upper part of Fig. 4, we show, as a function of the fragment mass A, the new position $Z_{prob}(A)$ of the ''residue corridor,'' for ^{129}Xe and ^{208}Pb, fragmentation. Data from ^{238}U fragmentation [20] are also included in the figure; they were not used to fit the parameters Δ_i and can serve as a check. For clarity, we plot the offset, Δ, from Z_β according to Eq. (5). The dashed lines are for EPAX version 1; the solid lines represent the new version 2. Note that for better results close to the projectile, we have added to Z_{prob} according to Eq. (5) a tiny fragment-mass dependent correction amounting to $0.002A$. The lines sloping downward above $A \approx 110$ and $A \approx 180$ illustrate the return of Z_{prob} to β stability close to the ^{129}Xe and ^{208}Pb projectiles according to Eq. (9).

In a similar way, the lower part of Fig. 4 visualizes the analytical description of the width parameter, R. While the functional form of the correction for Δ, Eq. (9), was kept identical with EPAX version 1, the correction for R near the projectile is now written as

$$R = R[1 + r_1 A_p (A/A_p - r_2)^4] \tag{14}$$

for $A/A_p \geqslant r_2$, which yields more narrow charge distributions for A close to A_p.

Only minor changes were introduced for the slope constants U_n and U_p of the neutron- and proton-rich sides of the charge distributions, respectively. While U_n was increased from 1.5 to 1.65 (constant for all A), U_p is now slightly fragment-mass dependent with

$$U_p = U_1 + U_2 A + U_3 A^2, \tag{15}$$

which approaches $U_p = 2.2$ for large A, compared to a previous constant value of 2.0 (Gaussian curve).

A close inspection of the width parameter R resulting from fits to the measured ^{86}Kr isotope distributions [5] shows that they are slightly but systematically decreased compared to Eq. (8) (see Fig. 4). This means that the isobar distributions are slightly wider for a neutron-rich projectile like ^{86}Kr than for a β-stable one. Therefore, we tentatively introduce the following neutron-excess dependence of R:

$$R' = R[1 - 0.0833(Z_{\beta p} - Z_p)], \tag{16}$$

where R is calculated according to Eq. (8). For neutron-deficient projectiles, R is not changed.

For a typical example, the combined effect of the changes described above is visualized in Fig. 5, which displays the isotope distributions from 800A MeV ^{129}Xe fragmentation measured over four orders of magnitude [6]. In particular, the data measured near the maximum are now much better reproduced. The stronger increase in R near the projectile mass, $A_p = 129$, leads to a much faster decrease of the corresponding fragment yields at $A \approx 124$. Similar observations, though over a smaller vertical range, can be made for the fragment distributions from ^{208}Pb fragmentation shown in Fig. 1. It is interesting to note that even for ^{238}U fragmentation products in the mass range $100 \lesssim A \lesssim 130$, produced in violent collisions and correspondingly long chains of statis-

tical evaporation, rather good agreement between experimental data [20] and EPAX can be observed.

B. Fragmentation of neutron- or proton-rich projectiles

In the previous EPAX version [10], the parametrization of the ''memory effect'' was fitted, for the case of neutron-rich projectiles, to the results from ^{48}Ca fragmentation at 213*A* MeV [2] [see Eq. (12)]. For the case of ^{86}Kr, we were able to check the validity of this prescription in a different fragment-mass range [5]. We have kept this prescription for the current version 2, since the agreement with experimental data has not changed significantly (see Fig. 6 for selected examples).

The situation is different, however, for the case of neutron-deficient projectiles. There, the previous version was unsatifactory from the beginning: First, there were only very few radiochemical cross sections available to derive a guess for the memory effect on the neutron-deficient side. Second, the resulting formula $\Delta_m=[p_2(A/A_t)^4](Z_p-Z_{\beta p})$ does not yield the limiting value $\Delta_m/(Z_p-Z_{\beta p})=1$ for $A=A_p$. These deficiencies became particularly obvious when Schneider *et al.* [16] measured only small cross sections for neutron-removal products from ^{112}Sn. This lead to a different functional form for the memory effect for neutron-deficient projectiles. The new parametrization reads

$$\Delta_m=\exp[p_1+p_2A/A_p](Z_p-Z_{\beta p}), \tag{17}$$

which is equivalent to a stronger but more rapidly decaying memory effect compared to the polynomial [Eq. (12)] used previously. The consequences of the new parametrization of the memory effect for neutron-deficient projectiles are visualized in Fig. 7. The small measured cross sections for ^{100}Sn [16] are now better reproduced, while the good agreement (over more than seven orders of magnitude) with data measured in ^{124}Xe fragmentation [21] is maintained.

We note in passing that Eq. (17) is very similar to what has been suggested by von Egidy and Schmidt [22] to reproduce production cross sections from antiproton annihilation. The overall agreement with the experimental fragmentation yields studied in our work is worse, however, when we adopt their description of the memory effect, in particular on the neutron-rich side. Moreover, we do not fit any set of parameters separately for a specific projectile as has been done in Ref. [22], but rather want to describe all systems with the same parameter set.

The yield distributions from the neutron-deficient projectile ^{58}Ni, studied in great detail by Blank *et al.* [4], deserve special attention. Not only do they represent a rare example of cross-section measurements down to the subnanobarn level, but also a case where severe discrepancies with EPAX version 1 were observed: the yields of even-*Z* isotopes close to the proton drip line where found to be enhanced in experiment by factors of up to 750 [4]. As a remedy for this deficiency, we have chosen to switch over from quasi-Gaussian to exponential slopes of the charge distribution above a certain gradient of the cross-section distribution. In order to achieve a steady transition between the two slopes, the transition point and the slope of the exponential have to be adjusted carefully. For this purpose, we calculate the derivative of the logarithm of the cross section [Eq. (1)]:

$$\frac{dF}{dZ}=\frac{d(\ln(\sigma))}{dZ}\approx\frac{-2R}{\ln(10)}(Z-Z_{prob}). \tag{18}$$

The transition point to the exponential slope, Z_{exp}, can be calculated for the proton-rich side as a function of the fragment mass *A* according to

$$Z_{exp}(A)=Z_{prob}(A)+\left.\frac{dF}{dZ}\right|_A\frac{\ln(10)}{2R(A)}. \tag{19}$$

From Z_{exp} on, the slope is exponential with the same gradient as Eq. (1) at this point.

The gradient for which we switch to the exponential slope has to be parametrized as a function of the fragment mass *A*. As for the moment only the ^{58}Ni data exhibit this exponential trend (the measured cross sections in the ^{100}Sn region reach the same cross section level, but are farther away from the proton drip line), we tried to adjust the function dF/dZ in such a way to reproduce the ^{58}Ni data without deteriorating the good agreement with the measured ^{124}Xe data. The function which fulfills reasonably well these criteria is the following:

$$\frac{dF}{dZ}=1.2+0.647(A/2)^{0.3}. \tag{20}$$

The result for the ^{58}Ni fragment-yield distributions is visualized in Fig. 8. The solid line shows the new EPAX cross sections including the above modification of the slopes, whereas the omission of the exponential slope leads to the dotted cross-section curve. As a consequence of this modification, EPAX version 2 predicts a production cross section, e.g., for the doubly magic nucleus ^{48}Ni of 4×10^{-13} b, which is within reach of an experiment.

As stated earlier, the present adjustment for very proton-rich projectile fragments is only based on results from ^{58}Ni fragmentation [4]. Therefore, caution is advisable when applying this parametrization especially to very light proton-rich fragmentation products. It would be interesting to compare the present parametrization to fragmention yields at the drip line from other proton-rich beams, e.g., from ^{36}Ar or ^{78}Kr. In the ^{100}Sn region, the present transition to an exponential slope has only a slight influence on the ^{100}Sn cross-section prediction from ^{112}Sn fragmentation (6.6×10^{-12} b, to be compared to an experimental value of 1.2×10^{-12} b [16]). It might be interesting to measure fragmentation cross sections for even more proton-rich nuclei in this mass region to compare to the modified EPAX formula.

C. Overall quality of EPAX version 2

Besides the comparison between experimental data and EPAX predictions for individual elemental distributions, we tried also to visualize in a more global manner the overall quality of the new EPAX parametrization compared to the data and the improvements with respect to EPAX version 1.

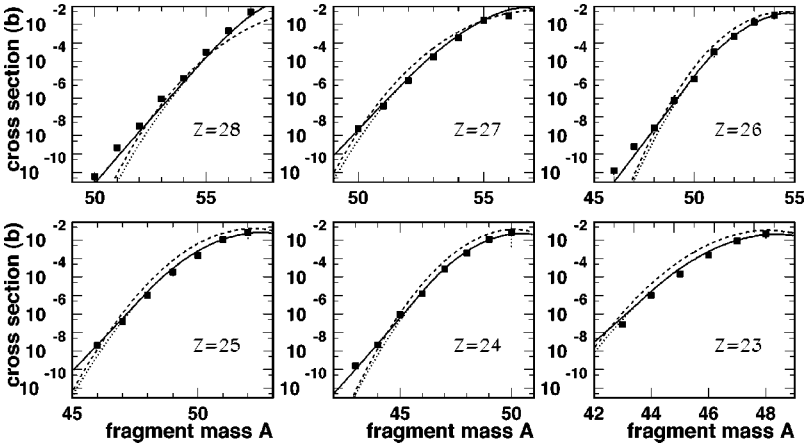

FIG. 8. Experimental isotope distributions for Ni to V isotopes from ^{58}Ni+^{9}Be fragmentation [4] in comparison with the old EPAX parametrization (dashed curves) and the new version (solid curves). The new EPAX formula without a transition to the exponential slope is shown by the dotted curve. This effect is clearly visible below the 10 nb level.

For this purpose, we plot the cross section ratios $\sigma_{exp}/\sigma_{\mathrm{EPAX}}$ for all projectile-target combinations used in the present paper in Fig. 9. For most of the projectiles the logarithm of the cross-section ratio is centered around zero, indicating an agreement on average between experiment and prediction. For the new EPAX version 2, the sigma widths of these distributions vary between 0.5 (in the case of ^{40}Ar and ^{86}Kr) and 0.2 (in the case of ^{129}Xe). If we analyze all experimental data together, we obtain a sigma of 0.4. This demonstrates that the new EPAX formula can predict cross sections in most cases within a factor of 2. In almost all cases we observe a significantly smaller sigma for the new EPAX parametrization than for the old version. This is particularly striking in the cases of ^{58}Ni, ^{129}Xe, and ^{208}Pb. Only in the case of ^{48}Ca does the agreement between experimental data and predictions deteriorate slightly, exhibiting now a shift to smaller predicted cross sections. It is likely that the memory effect for neutron-rich projectiles is the origin of this discrepancy.

D. Comparison with other empirical parametrizations

As has been mentioned in the Introduction and discussed in detail in Ref. [10], other empirical parametrizations have been proposed, mainly for proton-induced spallation reactions (e.g., Refs. [23,24]). Contrary to our formula, these parametrizations fit also the energy dependence of the cross sections. The former approach has been extended to describe heavy-ion induced spallation reactions by scaling proton-induced cross sections by an energy-dependent factor [25] and has achieved good agreement with measured cross sections (in the 100 mb to 1 mb range) for fragments from medium-mass nuclei (i.e., for projectiles up to ^{56}Fe [25]).

For fragmentation cross sections from heavy-mass nuclei, however, the formula of Tsao *et al.* [25] is less successful. This can be demonstrated, e.g., by comparing in Fig. 10 their prediction for the Pt isotope distribution in the reaction ^{208}Pb+^{nat}Cu to experimental data [7]. As we have mentioned in the Introduction, our physical understanding of high-energy heavy-ion reactions suggests that proton-induced reactions produce more neutron-rich isotope distributions of heavy elements than heavy-ion-induced reactions; therefore it is unlikely that even a better fit of the formula of Tsao *et al.* to the data in Fig. 10 would apply also to the same isotope distribution formed in the $p+^{208}$Pb reaction. We believe that separate parameter sets have to be fitted to the respective experimental data. For $\approx 1A$ GeV protons im-

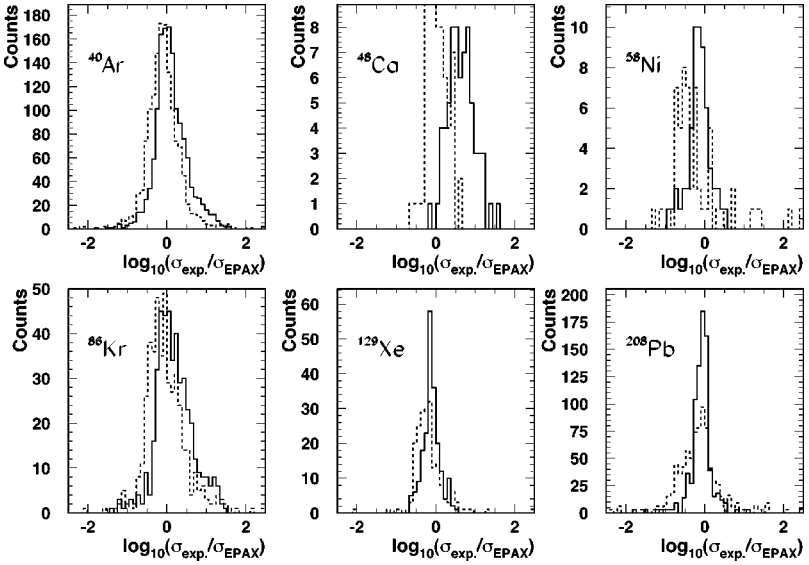

FIG. 9. Logarithm of the ratio between experimental fragmentation cross sections and predictions of EPAX version 1 (dashed line) and the new EPAX version 2 (solid line) for projectiles ranging from ^{40}Ar to ^{208}Pb. References to the experimental data are given in the text.

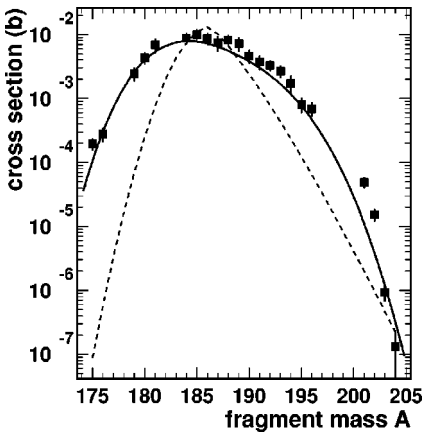

FIG. 10. Platinum ($Z=78$) isotope distribution from 1*A* GeV ^{208}Pb fragmentation in a ^{nat}Cu target [7] in comparison with the new EPAX parametrization (solid curve) and the formula of Tsao *et al.* (Ref. [25], dashed curve).

pinging on heavy targets, the recent work of Refs. [13,14] provides for the first time a comprehensive data set that allows to extend previous work [23,24] to heavier fragments. A complete parametrization of the bombarding-energy dependence, however, has to await more measurements at different energies for the heavy systems.

E. EPAX predicitions for projectiles very far from stability

The parameters of the new EPAX formula have been adjusted by fitting data from stable projectiles. As explained above, one of the most difficult tasks of the present work was to reasonably parametrize the cross sections for fragments close to the projectile. If the projectile is very far from the line of β stability, this task is even more difficult.

The comparisons between EPAX predictions and experimental data shown in the present paper indicate that the chosen parametrization is reasonable. A possible check of its predictive power could be to compare the EPAX formula to other data from neutron-rich or neutron-deficient projectiles. However, only very few other high-quality data are available.

As one check, we compare in Fig. 11 the fragmentation of a stable ^{24}Mg beam [18] to a radioactive ^{28}Mg beam [26] and of a stable ^{40}Ar beam [1] to a radioactive ^{43}Ar beam [26]. The elemental distributions for Mg, Na, and Ne isotopes shown in the left-hand column and those for S, P, and Si isotopes shown in the right-hand column nicely show the experimental memory effect and the high quality of the EPAX predictions. In a similar way we compared the results from fragmentation of ^{96}Ru and ^{96}Zr [27] to EPAX predictions and found reasonable agreement. However, for projectile beams still further away from stability, the memory effect becomes more and more important. Therefore, we think that some caution should be applied when using EPAX predictions for projectiles very far from stability like, e.g., ^{132}Sn. Here, no experimental data at all exist to verify the EPAX predictions.

IV. SUMMARY AND CONCLUSIONS

We have demonstrated that the quality with which EPAX reproduces measured high-energy fragmentation cross sections could be improved considerably by introducing rather small modifications to the formula. This makes EPAX a more reliable tool to predict production rates for secondary-beam experiments with medium- or heavy-mass exotic nuclei.

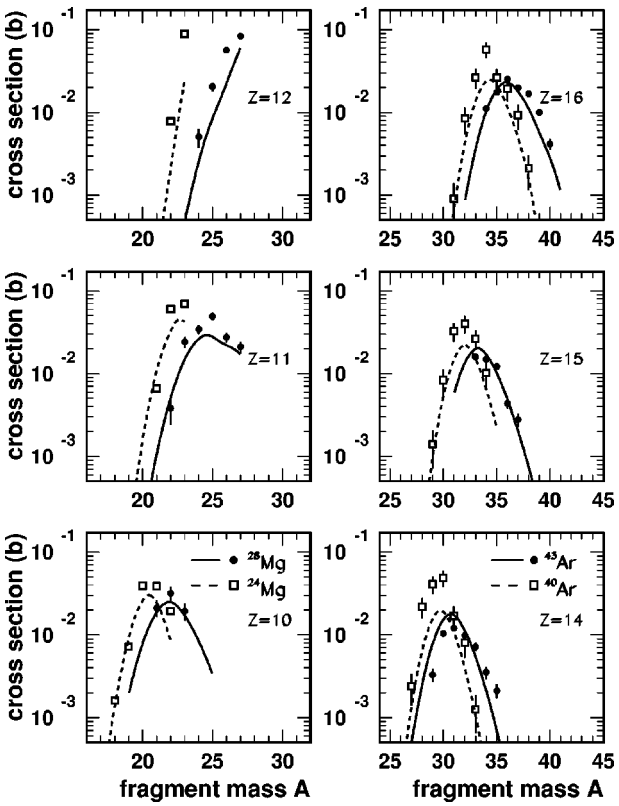

FIG. 11. Experimental cross sections for the fragmentation of stable (open symbols) and radioactive beams (solid symbols) compared to the new EPAX parametrization (dashed and solid lines, respectively). On the left-hand side, results from ^{24}Mg [18] and ^{28}Mg [26] fragmentation are shown, whereas on the right-hand side ^{40}Ar [1] fragmentation is compared to ^{43}Ar [26] fragmentation.

Even after introducing these improvements, there are still some discrepancies with measured data which deserve attention in future modifications of the EPAX formula. One aspect concerns the odd-even effects which were taken into account by von Egidy and Schmidt [22]. At present, we do not think that such a rather small modification (of the order of 20–30 %) is necessary in view of the overall discrepancies of factors around 2 still observed, but it may become necessary once better precision can be achieved. Another open question is the change in slope observed for very neutron-deficient ^{58}Ni fragmentation products. Here it would be desirable to measure systematically the formation cross sections for fragments close to the proton drip line for other medium-mass neutron-deficient projectiles, e.g., ^{36}Ar and ^{78}Kr.

Up to now, we did not use medium-energy data (from reactions at less than $\approx 100A$ MeV) which are available from GANIL, RIKEN, or MSU. First of all, these data probably do not fulfill the condition of ''limiting fragmentation'' mentioned above. In fact, it is well known that at these energies nucleon-exchange reactions as well as pickup reactions become increasingly important and thus alter in particular the cross sections close to the projectile. A striking example for

this is the difference in experimental cross sections for ^{100}Sn production from a ^{112}Sn beam of roughly a factor of 100 in recent GANIL and GSI experiments [21,28]. In addition, these intermediate-energy data are measured with separators having very low transmissions (of the order of a few percent) which are difficult to measure experimentally. It would be interesting, however, to compare EPAX also to cross sections obtained at lower incident energies once high-quality data become available.

A FORTRAN program of the EPAX formula as well as additional graphs comparing experimental data to EPAX predictions can be downloaded from the following address: ftp://ftpcenbg.in2p3.fr/pub/nex/epax

ACKNOWLEDGMENTS

We wish to thank our colleagues Jose Benlliure, Roman Gernhäuser, Manuel DeJong, Akira Ozawa, Jörg Reinhold, Robert Schneider, Shuying Wan, and Martin Weber for providing their experimental cross sections prior to publication. One of us (K.S.) acknowledges the kind hospitality of the Centre d'Études Nucléaires at Bordeaux-Gradignan where part of this work was completed.

[1] Y.P. Viyogi *et al.*, Phys. Rev. Lett. **42**, 33 (1979).
[2] G.D. Westfall *et al.*, Phys. Rev. Lett. **43**, 1859 (1979).
[3] H. Geissel *et al.*, Nucl. Instrum. Methods Phys. Res. B **70**, 286 (1992).
[4] B. Blank *et al.*, Phys. Rev. C **50**, 2398 (1994).
[5] M. Weber *et al.*, Nucl. Phys. **A578**, 659 (1994).
[6] J. Reinhold, J. Friese, H.-J. Körner, R. Schneider, K. Zeitelhack, H. Geissel, A. Magel, G. Münzenberg, and K. Sümmerer, Phys. Rev. C **58**, 247 (1998).
[7] M. DeJong *et al.*, Nucl. Phys. **A628**, 479 (1998).
[8] J.A. Winger *et al.*, Nucl. Instrum. Methods Phys. Res. B **70**, 380 (1992).
[9] N. Iwasa, H. Geissel, G. Münzenberg, C. Scheidenberger, T. Schwab, and H. Wollnik, Nucl. Instrum. Methods Phys. Res. B **126**, 284 (1997).
[10] K. Sümmerer, W. Brüchle, D.J. Morrissey, M. Schädel, B. Szweryn, and Yang Weifan, Phys. Rev. C **42**, 2546 (1990).
[11] G. Rudstam, Z. Naturforsch. A **21**, 1027 (1966).
[12] R. Silberberg and C.H. Tsao, Astrophys. J., Suppl. **25**, 315 (1973); **25**, 335 (1973).
[13] F. Farget *et al.*, in *Proceedings of the XVI EPS Nuclear Physics Division Conference (SNEC 98)*, Padova, 1998, edited by S. Lunardi, R.A. Ricci, and W. von Oertzen (Ed. Compositori, Bologna, 1998), p. 1097.
[14] W. Wlazlo *et al.*, in *Proceedings of the XXXVII International Winter Meeting on Nuclear Physics*, Bormio, Italy, 1998, edited by I. Iori (University of Milano, Milano, 1998), p. 321.
[15] J. Benlliure, A. Grewe, M. de Jong, K.-H. Schmidt, and S. Zhdanov, Nucl. Phys. **A628**, 458 (1998).
[16] R. Schneider *et al.*, GSI Scientific Report 1998, Report GSI-99-1, 1999, p. 19.
[17] A. Ozawa *et al.*, GSI Scientific Report 1998, Report GSI-99-1, 1999, p. 29.
[18] W.R. Webber, J.C. Kish, and D.A. Schrier, Phys. Rev. C **41**, 547 (1990).
[19] W.R. Binns, T.L. Garrard, M.H. Israel, M.P. Kertzmann, J. Klarmann, E.C. Stone, and J.C. Waddington, Phys. Rev. C **36**, 1870 (1987).
[20] J. Benlliure *et al.*, Eur. Phys. J. A **2**, 193 (1998).
[21] R. Schneider *et al.*, Z. Phys. A **348**, 241 (1994).
[22] T. von Egidy and H.H. Schmidt, Z. Phys. A **341**, 79 (1991).
[23] R. Silberberg, C.H. Tsao, and A.F. Barghouty, Astrophys. J. **501**, 911 (1998).
[24] W.R. Webber, J.C. Kish, and D.A. Schrier, Phys. Rev. C **41**, 566 (1990).
[25] C.H. Tsao, R. Silberberg, A.F. Barghouty, L. Shiver, and T. Kanai, Phys. Rev. C **47**, 1257 (1993); R. Silberberg, C.H. Tsao, and A.F. Barghouty, Astrophys. J. **501**, 911 (1998).
[26] Shuying Wan, Ph.D. thesis, University of Heidelberg, 1999.
[27] R. Gernhäuser, Ph.D. thesis, TU München, 1997.
[28] M. Lewitowicz *et al.*, Phys. Lett. B **332**, 20 (1994).